Received: 21 July 2023 | Revised: 12 March 2024 | Accepted: 29 May 2024

DOI: 10.1002/cyto.a.24856

ORIGINAL ARTICLE

MIFlowCyt

ISAC INTERNATIONAL SOCIETY FOR ADVANCEMENT OF CYTOMETRY

CYTOMETRY Journal of Quantitative Cell Science PART A

Unbiased method for spectral analysis of cells with great diversity of autofluorescence spectra

Janna E. G. Roet[1,2] | Aleksandra M. Mikula[1,2] | Michael de Kok[1,2,3] | Cora H. Chadick[1,2,3] | Juan J. Garcia Vallejo[1,2,3] | Henk P. Roest[4] | Luc J. W. van der Laan[4] | Charlotte M. de Winde[1,2,5] | Reina E. Mebius[1,2]

[1]Department of Molecular Cell Biology and Immunology, Amsterdam UMC location Vrije Universiteit Amsterdam, Amsterdam, The Netherlands

[2]Amsterdam Institute for Immunology and Infectious Diseases, Amsterdam, The Netherlands

[3]Microscopy and Cytometry Core Facility, Amsterdam UMC location Vrije Universiteit Amsterdam, Amsterdam, The Netherlands

[4]Department of Surgery, Erasmus MC Transplant Institute, University Medical Center Rotterdam, Rotterdam, The Netherlands

[5]Cancer Biology and Immunology, Cancer Center Amsterdam, Amsterdam, The Netherlands

Correspondence
Reina E. Mebius and Charlotte M. de Winde, Department of Molecular Cell Biology and Immunology, Amsterdam UMC location Vrije Universiteit Amsterdam, Boelelaan 1117, Amsterdam, The Netherlands.
Email: r.mebius@amsterdamumc.nl and c.m.dewinde@amsterdamumc.nl

Funding information
Dutch Research Council (NWO); Institute for Chemical Immunology, Grant/Award Number: 024.002.009; NWO ZonMw TOP, Grant/Award Number: 91217014; Cancer Center Amsterdam, Grant/Award Numbers: CCA2019-9-57, CCA2020-9-73; KWF Kankerbestrijding, Grant/Award Number: 2022-4 EXPL/14641; Convergence Health Technology Flagship; Medical Delta program

Abstract

Autofluorescence is an intrinsic feature of cells, caused by the natural emission of light by photo-excitatory molecular content, which can complicate analysis of flow cytometry data. Different cell types have different autofluorescence spectra and, even within one cell type, heterogeneity of autofluorescence spectra can be present, for example, as a consequence of activation status or metabolic changes. By using full spectrum flow cytometry, the emission spectrum of a fluorochrome is captured by a set of photo detectors across a range of wavelengths, creating an unique signature for that fluorochrome. This signature is then used to identify, or unmix, that fluorochrome's unique spectrum from a multicolor sample containing different fluorescent molecules. Importantly, this means that this technology can also be used to identify intrinsic autofluorescence signal of an unstained sample, which can be used for unmixing purposes and to separate the autofluorescence signal from the fluorophore signals. However, this only works if the sample has a singular, relatively homogeneous and bright autofluorescence spectrum. To analyze samples with heterogeneous autofluorescence spectral profiles, we setup an unbiased workflow to more quickly identify differing autofluorescence spectra present in a sample to include as "autofluorescence signatures" during the unmixing of the full stained samples. First, clusters of cells with similar autofluorescence spectra are identified by unbiased dimensional reduction and clustering of unstained cells. Then, unique autofluorescence clusters are determined and are used to improve the unmixing accuracy of the full stained sample. Independent of the intensity of the autofluorescence and immunophenotyping of cell subsets, this unbiased method allows for the identification of most of the distinct autofluorescence spectra present in a sample, leading to less

confounding autofluorescence spillover and spread into extrinsic phenotyping markers. Furthermore, this method is equally useful for spectral analysis of different biological samples, including tissue cell suspensions, peripheral blood mononuclear cells, and in vitro cultures of (primary) cells.

KEYWORDS
autofluorescence, data analysis, dimensional reduction, heterogeneity, spectral flow cytometry, spectral unmixing, unbiased clustering

1 | INTRODUCTION

Autofluorescence is an intrinsic factor of cells that is caused by the natural emission of light by its photo-excitatory molecular content, which can complicate analysis methods in which fluorescence is used, such as imaging and flow cytometry [1–9]. Different samples can have variable autofluorescence signatures, which can depend on many factors including cell type, metabolic state, sample preparation, and staining protocols, which can result in samples containing a heterogeneous autofluorescence profile [10]. In addition, autofluorescence has been described as a reliable in vitro marker of cellular senescence and aging in several cell types, including human mesenchymal stromal cells [11], human nerve cells [12], human skin, [13] and nematodes of *Caenorhabditis elegans* (*C. elegans*) [14]. As such, aged cells in vitro have increased autofluorescence.

Spectral flow cytometry is a powerful technology for cellular multiparameter analysis, in which mathematical algorithms are used to derive the expression on a per cell basis of specific markers, using the pure spectral signatures of fluorescently-labeled antibodies against these markers in a process called spectral unmixing [15]. Furthermore, this technology allows us to fully characterize autofluorescence heterogeneity within a sample, that is created by the different autofluorescence signatures of every cell within that sample [10].

In comparison to conventional flow cytometry, spectral flow cytometry captures the spectral profile of fluorochromes and autofluorescence by an array of detectors over multiple lasers that covers a wide range of emission wavelengths. However, spectral gaps are present in the array of detectors, that are associated with each laser path to reduce optical noise. Currently, most spectral flow cytometry software packages identify one autofluorescence signature per sample, allowing to distinguish between autofluorescence and fluorochrome signal [15,16]. However, when samples have a heterogeneous autofluorescence profile, it is challenging to resolve the spectra of all fluorochromes using the automated tools of the software, due to similarities between multiple autofluorescence spectra and some fluorochromes within one sample. A solution for this would be to add the different autofluorescence spectra as new references (single-spectra controls) to the unmixing. Indeed, it has been shown that addition of one autofluorescence spectrum for a bright autofluorescence cell subtype, namely alveolar macrophages within in a murine lung cell suspension, was able to reduce the autofluorescence signal and improve the fluorochrome signals [17]. However, when more cell types are present, identifying all cell types with their own unique autofluorescence spectra becomes a time consuming task. The solution for this would be to quickly identify every unique autofluorescence spectrum and add them to the downstream analysis.

A suggested workflow to identify unique autofluorescence subsets of cells would be to visualize unstained cells in a N × N matrix across all raw fluorescent detectors [10,16]. Sequential manual gating of cells with different autofluorescence spectra in a bivariate manner and evaluation of their uniqueness would result in identifying some unique autofluorescence subsets. However, this laborious approach is subjective, requires a certain level of expertise and can only be used if the autofluorescence subsets are abundantly present and therefore can be visually detected [10]. Moreover, autofluorescence subsets can easily be missed as the number of dimensions to check makes it complicated to capture all autofluorescence subsets manually. Therefore, this current method is not sufficient for all types of samples, especially when containing many different autofluorescence spectra. Dimensional reduction of the unstained sample based on the signal intensity within the different detectors of a spectral flow cytometer can be used as an alternative approach. This will result in a bivariate plot (e.g. Opt-SNE) displaying heterogeneity based on intrinsic autofluorescence [17]. Although this method helps to visualize different autofluorescence subsets, it still relies on selecting and gating the cells of interest manually.

Here, we provide an optimized approach to identify all different autofluorescence signatures within an unstained sample by including an unbiased clustering. Next, unique autofluorescence spectra are identified based on their similarity index (SI) and mean fluorescence intensity (MFI), which are subsequently used in the unmixing algorithm to extract the autofluorescence signal and improve the fluorochrome signal. We show that this approach is beneficial for various types of samples, including tissue cell suspensions with both heterogeneous and bright autofluorescence spectra (e.g., human lymph node cell suspensions), cells grown in vitro with extremely bright autofluorescence spectra (e.g., human fibroblastic reticular cells [FRCs]), and also (primary) cell suspensions with heterogeneous and dim autofluorescence spectra (e.g., peripheral blood mononuclear cells [PBMCs]). Using this methodology, we identified that the unique autofluorescence spectra differ between donor samples and over time in one cell type upon culturing, highlighting the importance of following this workflow with every analysis for identification of the unique autofluorescence spectra in a sample in order to improve spectral data analysis and interpretation.

2 | MATERIALS AND METHODS

2.1 | Samples

Human lymph nodes were obtained from donors during liver transplant procedures performed at the Erasmus MC, Rotterdam, the Netherlands. The use of these tissues was approved by the medical ethical committee of the Erasmus MC (MEC-2014-060) and the liver transplant recipients provided written informed consent for the use of samples. Donor characteristics are included in Table S1. Lymph nodes were transported in Belzer UW cold storage solution (UW, Bridge to Life) on ice and processed within 72 h after surgery. Lymph node cell suspensions were obtained through enzymatic tissue digestion as described previously [18]. In short, lymph nodes were digested using RPMI-1640 supplemented with 2.4 mg/mL Dispase II, 0.6 mg/mL Collagenase P, and 0.3 mg/mL DNase I (all from Sigma–Aldrich) for four rounds of 10 min at 37°C. After each round, the isolated cells were washed in ice cold phosphate buffered saline (PBS) supplemented with 2% FCS and 5 mM EDTA to stop the enzyme reaction and prevent over-digestion. Next, the cells were spun down at 300 × *g* for 4 min (4°C), the cell pellet was resuspended in 1 mL DMEM with 10% FCS and passed through a 100 µm filter.

PBMCs were isolated from buffy coats obtained from healthy donors (Sanquin, The Netherlands) by density gradient centrifugation with Ficoll-Paque PLUS (GE Healthcare). No donor specific information is provided.

2.2 | Cell culture

Lymph node cell suspensions were plated at a minimum cell concentration of 20 × 10^6 cells in a T-25 flask at 37°C, 5% CO_2. To grow out FRCs, flasks were pre-coated with 2 µg per cm^2 using a solution of 50 µg/mL collagen from calf skin in HBSS (Sigma–Aldrich) and the cells were grown in DMEM supplemented with 10% FCS, 2% penicillin/streptomycin/glutamine, and 1% Insulin-Transferrin-Selenium (Gibco). After 3 days, lymphocytes were washed away with PBS in order to allow stromal cell growth. Once confluent, FRCs were harvested with 0.5% trypsin + 5 mM EDTA and passaged or used for flow cytometry.

2.3 | CD45$^-$ stromal cell enrichment

Lymph nodes were digested as described above and enriched for CD45$^-$ stromal cells by negative selection using MojoSort™ Human CD45 Nanobeads (Biolegend). CD45$^-$ cell enrichment was performed according to manufacturer's protocol, with the addition of a fluorochrome-labeled antibody against CD45 (Table 1) during the CD45 Nanobeads incubation step to allow optimal CD45 fluorescent signal for flow cytometry.

2.4 | Flow cytometry

Cell suspensions were stained in a 96-well U bottom plate at 4°C for flow cytometric analysis. Cells were first washed with FACS buffer containing PBS + 1% FCS, then washed with PBS and stained with a fixable viability dye (Table 1) for 10 min at 4°C. Fc-receptor blocking was performed using 10% normal human serum. After brief centrifugation of the antibody stocks, the antibodies were diluted to the desired concentration in 1:1 FACS buffer and Brilliant Stain Buffer (BD Horizon) (Table 1). The cells were then incubated with these fluorochrome-labeled antibodies for 20 min at 4°C. After staining, cells were fixed with 2% PFA in PBS for 15 min, washed, resuspended in FACS buffer and acquired on a 5 Laser Aurora spectral analyzer (Cytek Biosciences, Fremont CA) with standard manufacturer optical configuration. For appropriate autofluorescence spectra detection and unmixing, an unstained sample was taken along during the procedure, that was treated according to exactly the same procedure as the

TABLE 1 Antibodies used for flow cytometry.

Fluorochrome	Target	Dilution	Species	Clone	Cat. no.	Manufacturer
Live/Dead Blue	Live/Dead Blue	1000	n/a	n/a	L34961	Invitrogen
BV421	CD106 (VCAM1)	200	Mouse	STA	305,816	Biolegend
eFluor450	CD45	100	Mouse	HI30	48–0459-42	Invitrogen
eFluor450	CD235a (Glycophorin A)	10	Mouse	HIR2	48–9987-42	Invitrogen
BV605	CD31 (PECAM-1)	100	Mouse	WM59	303,122	Biolegend
BV650	CCRL1 (ACKR4)	100	Mouse	13E11	747,804	BD Biosciences
BV711	CD146 (MCAM)	100	Mouse	P1H12	361,032	Biolegend
BV785	CD90 (Thy1)	100	Mouse	5E10	328,142	Biolegend
PerCP-Cy5.5	CD271 (NGFR)	100	Mouse	ME20.4	345,112	Biolegend
PE-Dazzle594	CD21 (CR2)	50	Mouse	Bu32	354,922	Biolegend
PE-Cy7	CD34	100	Mouse	581	343,516	Biolegend
Alexa Fluor 647	PDPN	50	Rat	NC-08	337,008	Biolegend

stained sample, of which at least the same amount of cells as in the stained sample were acquired. UltraComp eBeads compensation beads (Invitrogen) were used as single stain controls for the same fluorochrome-labeled antibodies as used in the panel, and the unstained beads were matched with the stained beads. Cells heat shocked for 3 min at 65°C were taken along as single stain control for the viability dye. All single stain controls were treated according to exactly the same procedure as the stained sample, except for the Fc-receptor blocking step.

2.5 | Data analysis

All autofluorescence spectra in an unstained sample were visualized and identified by performing dimensional reduction (Opt-SNE) and clustering (PhenoGraph) using the online software OMIQ (www.omiq.ai). The raw FCS file of the unstained sample was loaded into OMIQ, data cleanup was performed using PeacoQC for all features (settings: Maximum allowed median absolute deviations: 6; Isolation tree gain limit: 0.6; Maximum number of consecutive bins: 5; and Time units per visualization bin: 100) and all detectors were scaled to 6000 Arcsinh, the default scaling setting in OMIQ. Next, Opt-SNE (settings: Max iterations: 1000; Opt-SNE End: 5000; Perplexity: 30; Theta: 0.5; Components: 2; Random Seed: 6203; and Verbosity: 25), and PhenoGraph (settings: K nearest neighbors: 20; Distance metric: Euclidean; Louvain seed: 799; Louvain runs: 1; and Number of results: 1), were calculated for all events based on all 64 detectors of the Aurora 5L. The identified PhenoGraph clusters were gated and exported as one raw FCS file for all original features, excluding the opt_sne1, opt_sne2, and pgrahp features, and including all gates for the selected filters. The R-script "OMIQ-FCS-Separate" was used to split this file into separate FCS files per cluster. These files were used in a new experiment in SpectroFlo® to determine the similarity scores, by comparing the normalized spectra of all autofluorescence signatures. For this, a new fluorochrome library was created in SpectroFlo® containing all different "autofluorescence signatures", instead of fluorochromes. A reference group was assembled into a new experiment including an additional negative control and the "autofluorescence signatures" corresponding with the number of autofluorescence clusters. An unstained control with an autofluorescence signal close to the background of the instrument was generated by acquiring 30% Contrad® 70 (Decon). This unstained control was imported into the unstained and negative control tubes. The different autofluorescence clusters were imported as additional "autofluorescence signatures" in the reference group, visually checked whether every cluster contained one pure spectrum and used in the unmixing algorithm to define their uniqueness by means of calculating the similarity matrix. This matrix shows the SI of two spectra, which is a score between 0 and 1 that measures how closely two normalized spectra match. The unmixing algorithm of SpectroFlo®, that uses the ordinary least squares, can unmix the sample when this number is ≤0.98 and there are at least 300 events per spectrum [16,19]. To identify the unique autofluorescence spectra, the similarity matrix was analyzed by the R-script "SpectroFlo-Find-Unique-Spectra." Herein, the unique spectra are determined based on a ranking of the number of firstly, similar spectra (SI >0.98) and secondly, the sum of SI per cluster. When two spectra have identical number of similar spectra and sum of SI, the spectrum with the highest MFI should be chosen. From every unique spectrum, the similar spectra (SI >0.98) are listed in the data table within R. By comparing the MFI per unique spectrum and its similar spectra in SpectroFlo®, the spectrum with the highest MFI can be chosen per unique spectrum. Make sure that the chosen spectra are not accidently similar to other chosen spectra (SI ≤0.98).

Next, the not unique autofluorescence spectra were eliminated and the unique autofluorescence spectra were used to unmix the raw data of the original experiment, including unstained and full stained samples. Unmixing was performed in SpectroFlo (version 3.0.3), on an analysis workstation with the instrument data backup. The corresponding autofluorescence spectra were added to the reference group together with an additional negative control, to correct for the background noise of the machine. Again, the negative control and unstained sample of the reference group were replaced with a FCS file containing events without any autofluorescence and unmixing was performed.

The addition of extra fluorochromes to the unmixing can reduce the resolution of some fluorochromes, due to overlap between the newly added autofluorescence signatures and the spectra of the actual fluorochromes, leading to spillover spread. To improve the resolution, but still resolve the autofluorescence, the unmixing was evaluated after the reduction of the different autofluorescence spectra (Figure S2). The autofluoresence spectra were removed one by one from lowest to highest uniqueness, as given by the order of the output of the unique spectra identified with the R-script "SpectroFlo-Find-Unique-Spectra," which is from most to least unique. After unmixing, the N × N plots of the unstained sample were evaluated to identify whether the removed autofluorescence spectrum was necessary to resolve all autofluorescence. If no autofluorescence was detected, this autofluorescence spectrum could be removed. However, if the autofluorescence was increased in the unstained sample for any of the fluorochromes, this autofluorescence spectrum could not be removed and was added back to the unmixing. Then, the next autofluorescence spectrum was removed from the unmixing and the whole procedure was repeated until all autofluorescence spectra were tested (Figure S2). After unmixing with the optimal number of autofluorescence spectra, live cells were gated (Figure S3) and subsequently spillover correction was performed using SpectroFlo®, based on the single color controls and the added autofluorescence spectra samples within the reference group.

Data is visualized using FCS express (De Novo Software) for the raw spectra and Prism (Graphpad Software) for the unique and normalized spectra and bar graphs. All other figures are produced using OMIQ (www.OMIQ.ai). For the density plots produced with OMIQ, data cleanup was performed using PeacoQC for all features (settings: Maximum allowed median absolute deviations: 6; Isolation tree gain limit: 0.6; Maximum number of consecutive bins: 5; and Time units per visualization bin: 100). Next, cells of interest were gated based on FSC and SSC (Figure S3). These unstained cells were used for Figures 2A and 4. For the stained cells used in Figures 2 and 3, viable cells were gated as cells that lacked the Live/Dead Blue staining

(Figure S3A). Scatter plots (density) with 5 number levels and 0.4 percentile outliers were used to visualize the data.

2.6 | Data availability statement

The R-scripts used in this manuscript are publicly available at https://github.com/MolecularCellBiologyImmunology/Autofluorescence-Workflow. The FCS files used in this manuscript are publicly available at http://flowrepository.org/id/FR-FCM-Z78C and are annotated in Table S4.

3 | RESULTS

3.1 | Determination of all unique autofluorescence subsets of cells using unbiased clustering

To correctly identify all autofluoresence spectra within a cell suspension for flow cytometric analysis, a workflow was created to identify all autofluorescence clusters present in a sample, with each cell cluster having its own unique autofluorescence spectrum (Figure 1A). First, the spectral profile of an unstained sample was acquired. To take into account autofluorescence induced during the preparation of the sample, the unstained sample had undergone the same wash-steps as the full stained sample. Furthermore, to be able to identify all different autofluorescence subsets, the same amount of events for the unstained sample as for the full stained samples was acquired.

To visualize and verify the different steps of the workflow that is presented in this paper, we used a freshly digested human lymph node cell suspension enriched for $CD45^-$ cells, as the lymph node contains different cell types including $CD45^-$ lymph node stromal cells, which tend to have highly heterogeneous and bright autofluorescence signatures. The signal intensities within the 64 detectors form a heterogeneous spectral profile in combination with high autofluorescence, with signals up to 10^6 for the ultra-violet, violet, and blue lasers (Figure 1B). The dimensional reduction Opt-SNE and clustering algorithm PhenoGraph visualized and identified 28 clusters based on the signals from the 64 different detectors (Figure 1C). Next, it is important to identify which of these clusters are unique, that is, have autofluorescence spectra that are different enough to be used by the unmixing algorithm. The similarity matrix, which is a measurement how closely spectra match, of all autofluorescence spectra is calculated in SpectroFlo® (Table S2) and the custom made R-script identified the unique spectra based on the ranking of the number of similar spectra (SI >0.98), the sum of SI per cluster and the MFI of the peak emission channel, as described before [10]. For this human lymph node cell suspension, eight unique autofluorescence clusters could be identified (Figure 1D,E). The unique autofluorescence clusters have spectral profiles with differences in brightness and with distinct normalized spectra (Figure S1A). Furthermore, the unique clusters could not all be distinguished based on FSC and SSC, but include clusters with low SSC (clusters 4, 8, and 20), suggesting immune cells, a cluster with low FSC (cluster 1), suggesting dead cells and clusters with intermediate to high SSC and FSC (clusters 13, 18, 19, and 21), suggesting stromal cells (Figure S1B).

3.2 | Improved unmixing by addition of unique autofluorescence spectra

Next, the identified unique autofluorescence spectra (Figure 1E) were used for unmixing by adding them as separate autofluorescence signatures in addition to the fluorochromes already present in the antibody panel. The highest similarity between the autofluorescence spectra and the fluorochromes is seen for BV605 and BV650, with similarity indices up to 0.77 (Table S3). Unmixing with additional eight unique autofluorescence spectra reduced the autofluorescence signal present in the unstained and stained sample for different fluorochromes (Figure 2A). This is observed for fluorochromes with peak emissions in the highly autofluorescence violet channels (BV605, BV711, and eFluor450), but also for fluorochromes with peak emissions overlapping with secondary emission channels from other fluorochromes (BV785 and PE-Cy7) or for fluorochromes with a peak emission in the less autofluorescence red channel (AF647) (Figure 2A). The $CD45^+$ population seen in the sample unmixed without autofluorescence spectra (Figure 2A, first row), is reduced upon unmixing with eight autofluorescence spectra (Figure 2A, second row), showing that some signal within this population was created by autofluorescence and not by true fluorochrome signal.

The addition of extra autofluorescence spectra to the unmixing also resulted in lower resolution of the fluorochrome signal markers (Figure 2A, second row). To improve the resolution of some markers while still resolving autofluorescence, we removed the autofluorescence spectra one by one from lowest to highest uniqueness (Figure S2). For this human lymph node cell suspension, the eight unique autofluorescence spectra could be reduced to five unique autofluorescence spectra without increasing the autofluorescence signal (Figure 2A, third row). In contrast, when the unmixing was reduced to four unique autofluorescence spectra, autofluorescence was again detected (Figure 2A, fourth row). The reduction from eight to five autofluorescence spectra during the unmixing especially improved the resolution of the fluorochrome BV711 in this sample (Figure 2B). After unmixing with five autofluorescence spectra, we performed spillover correction using single stained controls, which reduced the spread identified for some of the markers, especially PE-Cy7 versus BV785 and BV711 versus BV605 (Figure 3).

3.3 | Unbiased autofluorescence finding is beneficial for different types of samples

Identification of all unique autofluorescent spectra within a sample is beneficial for the unmixing of samples with both different cell populations, as well as cells with high autofluorescence, as seen for the human lymph node cell suspension (Figures 2,3). To test whether this workflow is also valuable for spectral flow cytometry analysis of cells with high autofluorescence in vitro, and for heterogeneous cell

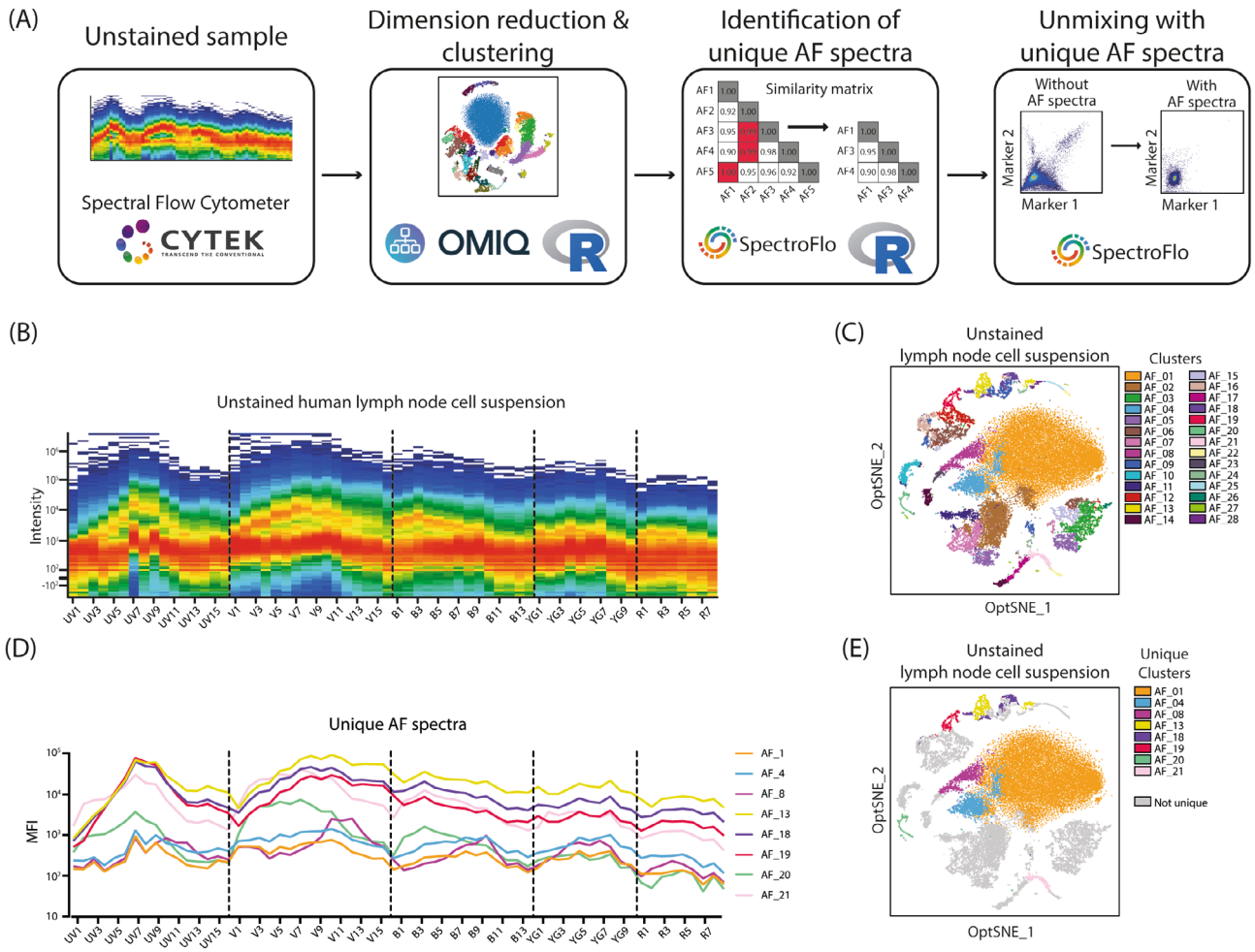

FIGURE 1 Identification of all unique autofluorescence spectra using dimension reduction and clustering. (A) Schematic representation of the workflow and software needed to identify all unique autofluorescence spectra within an unstained sample that can be used for unmixing. (B) Raw spectrum of an unstained human lymph node cell suspension acquired on Aurora 5 L. (C) Opt-SNE projection of all 28 autofluorescence clusters of the unstained human lymph node cell suspension. The Opt-SNE and PhenoGraph clusters were analyzed based on all 64 raw fluorescence detectors of the Aurora 5 L. (D) Spectra of the eight unique autofluorescence clusters of the unstained human lymph node cell suspension. The unique autofluorescence clusters were determined using the SI from SpectroFlo® and the R-script "SpectroFlo-Find-Unique-Spectra." (E) Opt-SNE projection of the eight unique autofluorescence clusters of the unstained human lymph node cell suspension. AF, autofluorescence; B, blue; MFI, mean fluorescent intensity; R, red; UV, ultraviolet; V, violet; YG, yellow green. [Color figure can be viewed at wileyonlinelibrary.com] [Color figure can be viewed at wileyonlinelibrary.com]

suspensions with low autofluorescence, we, respectively, analyzed FRCs and PBMCs. FRCs have extremely high autofluorescence, with signal up to 10^6 in the ultraviolet, violet, and blue channels and signal up to 10^5 in the yellow-green and red channels (Figure 4A-i). Within this sample of FRCs, six different unique autofluorescence spectra were identified (Figure 4A-ii). Addition of these six autofluorescence spectra to the unmixing reduced the autofluorescence signal from unstained cells from 10^4 to around 0 into different fluorochromes, including PE-Cy7 and BV785 (Figure 4A-iii). PBMCs have a heterogeneous spectral profile with autofluorescence signal up to 10^4 in the ultraviolet, violet, and blue channels (Figure 4B-i). Within this sample, four different unique autofluorescence spectra were identified (Figure 4B-ii). Addition of these four unique spectra to the unmixing reduced the autofluorescence signal in the unstained PBMCs in different fluorochromes, including eFluor450 and BV605 (Figure 4B-iii).

3.4 | Unique autofluorescence spectra differ between donor samples and within one cell type over time

The addition of one predefined autofluorescence spectrum per cell type has been shown to be beneficial for unmixing, for example, the addition of the alveolar macrophage autofluorescence spectrum to lung cell suspensions [17]. To identify whether this workflow can be used to create a library of unique autofluorescence spectra per sample or cell type that can be used for the unmixing of new samples of the same type, we compared the unique autofluorescence spectra found in different unstained samples. The unique autofluorescence spectra identified in lymph node cell suspensions of five different donors, which were processed and acquired on different days, except for donors three and four which were processed and acquired on the

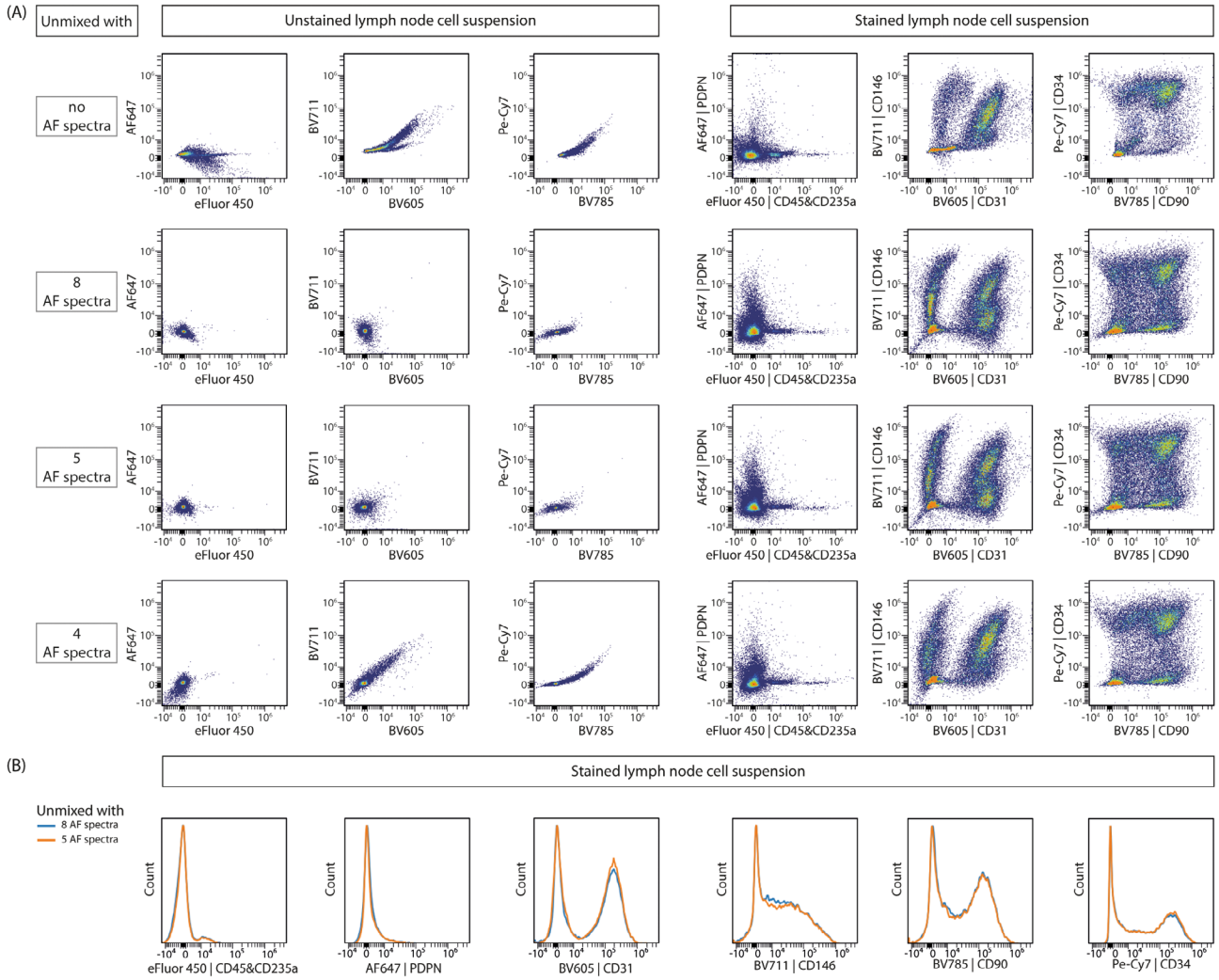

FIGURE 2 Unmixing of samples with or without the addition of autofluorescence spectra. (A) Scatter plots of the unstained lymph node cell suspension (left) and stained viable lymph node cell suspension (right), enriched for CD45$^-$ cells, after unmixing without autofluorescence extraction (first row), with the eight unique autofluorescence spectra (second row), with a reduced number of unique autofluorescence spectra, respectively, five (third row) and four (fourth row) autofluorescence spectra. The spectra were reduced one by one from lowest to highest uniqueness (Figure S2). (B) Histograms of the stained lymph node cell suspension after unmixing with eight (blue) or five (orange) unique autofluorescence spectra. For all plots, the fluorochromes visualized have peak emissions in the highly autofluorescence violet channels (eF450, BV605, and BV711), have peak emissions overlapping with secondary emission channels from other fluorochromes (BV785 and PE-Cy7), or have a peak emission in the less autofluorescence red channel (AF647). AF, autofluorescence, BV, brilliant violet. [Color figure can be viewed at wileyonlinelibrary.com] [Color figure can be viewed at wileyonlinelibrary.com]

same day, did not completely overlap between the donor samples (Figure 4C). The observed differences were not related to the sex or the age of the donor (age 16 versus 83, Table S1). Although some unique spectra did overlap between all five donors, four out of five donors also had unique autofluorescence spectra that were specific for that donor sample (Figure 4C). A similar pattern is seen when comparing the unique autofluorescence spectra identified from passage two until six of cultured FRCs from the same donor. Three out of five passages had autofluorescence spectra overlapping with all other passages (Figure 4D). However, they also contained unique autofluorescence spectra that were not identified in other passages (Figure 4D). These data show that unique autofluorescence spectra differ between donor samples and within one cell type over time in culture and that selecting predefined autofluorescence spectra per cell type will not be sufficient to cover all autofluorescence within a sample.

4 | DISCUSSION

Here we introduce an unbiased workflow for spectral flow cytometry to identify autofluorescence signatures in a variety of samples containing heterogeneous autofluorescence profiles. This method improves signal-to-noise ratio in spectral flow cytometry data, but is

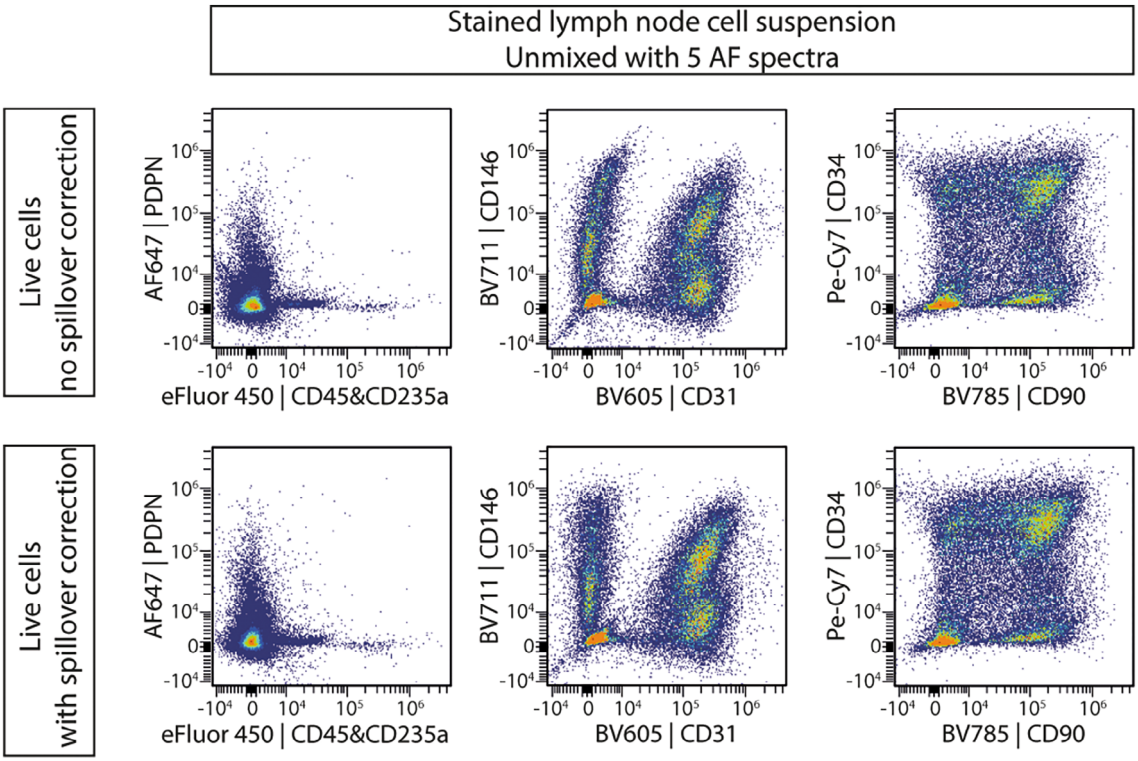

FIGURE 3 Reducing spread of samples unmixed with autofluorescence spectra by spillover correction. Scatter plots of the stained lymph node cell suspension unmixed with five autofluorescence spectra, gated on live cells (top) and the addition of spillover correction (bottom). Spillover correction was based on the single color controls and the added autofluorescence spectra samples within the reference group. For all plots, the fluorochromes visualized have peak emissions in the highly autofluorescence violet channels (eF450, BV605, and BV711), have peak emissions overlapping with secondary emission channels from other fluorochromes (BV785 and PE-Cy7), or have a peak emission in the less autofluorescence red channel (AF647). AF, autofluorescence, BV, brilliant violet. [Color figure can be viewed at wileyonlinelibrary.com] [Color figure can be viewed at wileyonlinelibrary.com]

also valuable for autofluorescence-based cell sorting. Our method entails first the identification of all autofluorescence subsets using dimensional reduction (Opt-SNE) and clustering (PhenoGraph), then evaluation and selection of unique autofluorescence spectra based on the similarity matrix, after which the autofluorescence signal is extracted by adding them to the unmixing algorithm.

Recently, a workflow was published which also used dimensional reduction to visualize different autofluorescence subsets, followed by the manual selection of cells with the highest autofluorescence spectrum [17]. We have now improved this workflow by replacing the manual gating with unbiased clustering and automated gating. The advantage of unbiased clustering is that this will select all subsets with unique autofluorescence spectra and not only the ones manually selected.

It has been shown that the addition of only one or two autofluorescence spectra to the unmixing algorithm could improve signal-to-noise ratios. For example, the addition of the autofluorescence spectrum of murine alveolar macrophages improved the unmixing of murine lung cell suspensions [17]. Also, the addition of both the autofluorescence spectra of lymphocytes and monocytes/neutrophils as separate spectra improved the unmixing output of human PBMCs [20]. In our study, we showed that unmixing accuracy could be improved by the addition of multiple autofluorescence spectra, demonstrating the importance of identifying all different unique autofluorescence spectra in a sample for the final analysis.

Besides the use of this workflow to improve signal-to-noise ratio, the identified unique autofluorescence signatures can also be used as a parameter on its own, when a proper and consistent sample preparation is performed. It has been shown that distinct autofluorescence spectra can be used to identify different cell subsets, for example, to distinguish hepatoblast-like cells and mature cholangiocytes within murine fetal livers [21]. Moreover, autofluorescence can be used as parameter for label-free sorting on conventional cell sorters, for instance of senescent cells from mesenchymal stromal cell cultures [22] or neutrophils from peripheral blood human granulocytes [23]. Combining high-end spectral cell sorters and the workflow presented in this paper could facilitate the sorting of different (unknown) cell subtypes purely based on their autofluorescence profile. Additionally, autofluorescence is a property of cells that reflects diversity in intracellular composition that may be linked to functional differences. It has been shown that the autofluorescence of human lymph node stromal cells of rheumatoid arthritis patients was significantly higher compared with healthy controls, which was in line with other senescence hallmarks (including increased DNA damage and lipofuscin positive granules), suggesting that autofluorescence contributes to functional changes in rheumatoid arthritis [24]. This

workflow can offer an enormous potential in future research to investigate metabolic and proteomic foundations of autofluorescence properties.

The workflow described in this paper is focused on the use of the Aurora spectral flow cytometer and the accompanied SpectroFlo® software from Cytek Biosciences. However, with the addition of some

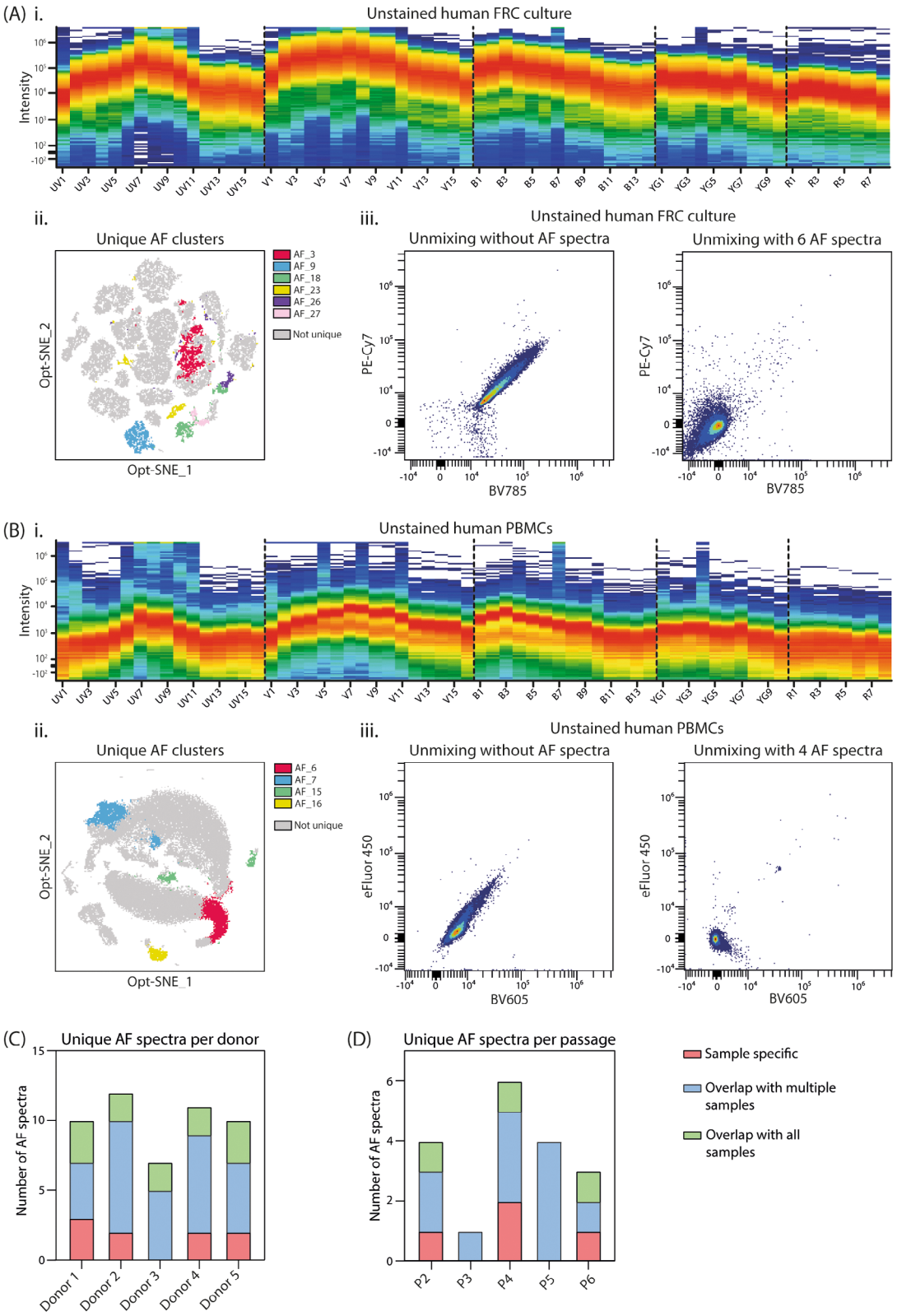

FIGURE 4 Legend on next page.

small adjustments this protocol can be used for different types of spectral flow cytometers. To do so, it is necessary that the raw spectrum profile can be exported and that additional spectra can be added to the unmixing algorithm. As the Cytek Similarity Index, which is a metric developed by Cytek Biosciences, is exclusive for the SpectroFlo® software, a matrix of Pearson r correlations could also be used for the identification of unique spectra when working with other software. In our hands (data not shown) and as described before [17], these two methods had an almost perfect linear correlation.

Some spectral flow cytometry software have incorporated a tool to take the autofluorescence spectrum of a sample into account during the unmixing. For example, the SpectroFlo® software can treat the autofluorescence spectrum of the sample, defined by gating on the cells of interest based on FSC and SSC, as a separate parameter and extracts it from the fluorescence data, if desired [10]. This can be used when the sample contains a single autofluorescence spectrum, as this spectrum is extracted from all cells within the sample. However, this tool is not sufficient to reduce all autofluorescence in samples with heterogeneous autofluorescence profiles. As this tool extracts the mean autofluorescence spectrum from a mixture of cells with all different autofluorescence profiles, it would result in photons from autofluorescence being wrongly assigned. This would impact the resolution between the fluorochromes, making the analysis less sensitive. Therefore, in a heterogeneous sample, it is necessary to identify all different autofluorescence subsets to use them in the unmixing algorithm.

The method described here is unbiased in identifying and selecting unique autofluorescence spectra. The only manual component described in our workflow is the reduction of the number of added autofluorescence spectra in the unmixing to improve the resolution of some fluorochromes. To make this workflow totally unbiased, a tool would need to be created that can evaluate the effectiveness of the different combinations of autofluorescence spectra used for unmixing. For example, by generating an unmixing score based on the signals for all the different fluorochromes within the unstained sample, especially by paying attention to the outliers and extreme negative values. This can then be used to evaluate in an unbiased setting whether the reduction of added autofluorescence spectra affects the unmixing accuracy.

Remarkably, we showed that unique autofluorescence spectra are present in similar tissue samples from different donors, including two donors processed on the same day, and even within cultures of the same cells over different passages. Therefore, we highlight that this method should be performed with every new acquired sample, to identify the unique autofluorescence spectra for that specific sample at that specific time. However, when the same sample types are used, an additional step can be added to the workflow to build an extensive library of all unique spectra identified that could not be removed and were thus necessary for correct unmixing accuracy. When enough samples are acquired, these spectra can be evaluated to identify whether there is a pattern of autofluorescence spectra that are always needed for correct unmixing. These spectra can then be beneficial for the unmixing of later experiments with the same sample types. Although such a pattern was not present for the lymph node cell suspensions and in vitro FRCs (Figure 4C,D), we hypothesize that such a pattern might be present in other samples, depending on the sample type, number of samples, preparation, and acquisition.

Besides the mathematical extraction of the autofluorescence signal after acquisition, reduction of the autofluorescence signal before acquisition is often used in fluorescent microscopy [25–27]. Various reagents have been described to quench autofluorescence signal. For example, Sudan Black B has been shown to eliminate autofluorescence on both frozen and paraffin embedded sections of multiple tissues [25,26]. We have explored whether these methods can also be applicable for flow cytometric analysis. Unfortunately, we noticed that Sudan Black B adds its own fluorescent spectrum to our flow cytometry samples, making it not useful for quenching autofluorescence in spectral flow cytometry (unpublished observations). Another method that has been described to reduce autofluorescence in microscopy is photobleaching using UV light, which induces irreversible modifications of fluorochromes [27]. This method has also been described to quench antibody-conjugated fluorochromes signal on live cells in suspension. To minimize viability loss, constant cooling and anti-oxidants are necessary to prevent reactive oxygen species from damaging cells [28]. Antibody-conjugated fluorochromes can be photobleached in 3–25 min. However, to quench autofluorescence a longer exposure time is needed: 24 h to multiple days have been described for microscopy [27]. Because a long exposure time to UV light would kill live, unfixed cells and quench fluorescent signals from antibody-conjugated fluorochromes, autofluorescence photobleaching could only be used for flow cytometry on fixed, unstained samples. This reduces its capacity as a general method to reduce autofluorescence in spectral flow cytometry. Overall, reduction of the autofluorescence before acquisition is not always feasible, and a simple way to get the best

FIGURE 4 Unbiased autofluorescence detection in different types of samples. (A) i. Raw spectrum of a sample of unstained human FRCs in culture acquired on Aurora 5 L. ii. Opt-SNE projection of the six unique autofluorescence spectrum identified in this sample. iii. Scatter plots after unmixing without autofluorescence or with the six unique autofluorescence spectra. (B) i. Raw spectrum of a sample of unstained human PBMCs acquired on Aurora 5 L. ii. Opt-SNE projection of the four unique autofluorescence spectrum identified in this sample. iii. Scatter plots after unmixing without autofluorescence or with the four unique autofluorescence spectra. (C) Count of the unique autofluorescence spectra in the human lymph node cell suspension of five different donors, divided into sample-specific (red), overlap with multiple samples (blue), or overlap with all samples (green). (D) Count of the unique autofluorescence spectra per passage of FRCs from the same donor in culture for five passages, divided into sample-specific (red), overlap with multiple samples (blue), or overlap with all samples (green). AF, autofluorescence; B, blue; BV, brilliant violet; FRC, fibroblastic reticular cell; P, passage; PBMCs, peripheral blood mononuclear cells; R, red; UV, ultraviolet; V, violet; YG, yellow green. [Color figure can be viewed at wileyonlinelibrary.com] [Color figure can be viewed at wileyonlinelibrary.com]

signal-to-noise ratio when working with autofluorescence samples is to assign the fluorochromes used within the antibody panel on forehand in such a way that they have the least overlap and interference with the autofluorescence spectrum of the unstained cells.

A limitation of working with samples with a heterogeneous autofluorescence profile is that these samples cannot be used as single stain controls during unmixing. The rule for single stain controls is that the positive and negative events should have the same autofluorescence [29]. In this article, we demonstrate that our sample does not have a homogeneous autofluorescence profile and can therefore not be used for single stain controls. Another rule for single stain controls is that the positive signal should be as bright or brighter than in the experimental sample [29]. Unfortunately, the positive signal on the compensation beads used as single stain controls was sometimes dimmer than in the experimental sample. This is an inherent limitation of this study, but we tried our best to minimize the impact on our work. We also tested SpectraComp beads (Slingshot), which could have a higher fluorescence intensity, but we observed that these were not always bright enough (Figure S4). For example, fluorescence intensities up to 10^6 were identified for CD90 BV785 in the lymph node cell suspension (Figure 2), while fluorescence intensities up to 3×10^4 on SpectraComp beads and 6×10^4 on UltraComp eBeads were present for CD90 BV785 (Figure S4). More research into and better reagents to optimized single stain controls are needed to go further in this field.

To summarize, we here describe an improved, unbiased method to identify and select all unique autofluorescence spectra using spectral flow cytometry. Addition of these spectra to the unmixing algorithm reduces the autofluorescence background and increases the resolution to detect different fluorochromes. This workflow is beneficial for spectral flow cytometry analysis of various types of samples, including samples containing very high autofluorescence signal and/or with a heterogeneous autofluorescence profile.

AUTHOR CONTRIBUTIONS

Reina E. Mebius: Conceptualization; methodology; writing – review and editing; supervision; funding acquisition. **Janna E. G. Roet:** Conceptualization; methodology; software; data curation; investigation; visualization; writing – original draft; writing – review and editing; formal analysis. **Aleksandra M. Mikula:** Methodology; investigation; data curation. **Michael de Kok:** Software. **Cora H. Chadick:** Methodology. **Juan J. Garcia Vallejo:** Conceptualization; methodology; writing – review and editing. **Henk P. Roest:** Writing – review and editing; resources. **Luc J. W. van der Laan:** Resources; writing – review and editing. **Charlotte M. de Winde:** Conceptualization; methodology; writing – review and editing; supervision.

ACKNOWLEDGMENTS

The authors would like to thank and acknowledge the expert help of the Microscopy and Cytometry Core Facility at Amsterdam UMC location Vrije Universiteit, Amsterdam. We thank Kim Ober and Dr. Monique Verstegen from the Erasmus Medical Centre, Rotterdam, for sample logistics, and Dr. Maria Jaimes from Cytek for the critical reading of the manuscript. We thank Biolegend for advice on initial antibody panel design, and Alberta Paul (Cytek) for advice on and help with improved and extended antibody panel design for multispectral flow cytometry of lymph node stromal cells.

FUNDING INFORMATION

JEGR is supported by a gravitation 2013 BOO grant financed by the Dutch Research Council (NWO) as part of the Institute for Chemical Immunology (ICI; 024.002.009). AMM is supported by the NWO ZonMw TOP grant (91217014). CMdW is supported by Cancer Center Amsterdam (CCA2019-9-57 and CCA2020-9-73) and the KWF Kankerbestrijding (KWF; 2022-4 EXPL/14641). LJWvdL is supported by funding from the Convergence Health Technology Flagship grant (Organ Transplantation) and Medical Delta program grant (Regenerative Medicine 4D).

CONFLICT OF INTEREST STATEMENT

The authors declare no conflicts of interest.

PEER REVIEW

The peer review history for this article is available at https://www.webofscience.com/api/gateway/wos/peer-review/10.1002/cyto.a.24856.

DATA AVAILABILITY STATEMENT

The R-scripts used in this manuscript are publicly available at https://github.com/MolecularCellBiologyImmunology/Autofluorescence-Workflow. The FCS files used in this manuscript are publicly available at http://flowrepository.org/id/FR-FCM-Z78C and are annotated in Table S4.

ORCID

Janna E. G. Roet https://orcid.org/0009-0009-6998-3723
Michael de Kok https://orcid.org/0000-0001-6652-2723
Juan J. Garcia Vallejo https://orcid.org/0000-0001-6238-7069
Luc J. W. van der Laan https://orcid.org/0000-0002-0651-5334
Charlotte M. de Winde https://orcid.org/0000-0002-8318-4612
Reina E. Mebius https://orcid.org/0000-0003-0451-7464

REFERENCES

1. Cardoso Dos Santos M, Colin I, Ribeiro Dos Santos G, Susumu K, Demarque M, Medintz IL, et al. Time-gated FRET nanoprobes for autofluorescence-free long-term in vivo imaging of developing zebrafish. Adv Mater. 2020;32(39):e2003912. https://doi.org/10.1002/adma.202003912
2. Celik-Uzuner S, O'Neill C. Cellular autofluorescence in mouse embryonic fibroblasts interferes with antigen detection using flow cytometry. J Fluoresc. 2021;31(3):873–9. https://doi.org/10.1007/s10895-021-02724-1
3. Duong H, Han M. A multispectral LED array for the reduction of background autofluorescence in brain tissue. J Neurosci Methods. 2013;220(1):46–54. https://doi.org/10.1016/j.jneumeth.2013.08.018
4. Mosiman VL, Patterson BK, Canterero L, Goolsby CL. Reducing cellular autofluorescence in flow cytometry: an in situ method. Cytometry. 1997;30(3):151–6. https://www.ncbi.nlm.nih.gov/pubmed/9222101
5. Neumann M, Gabel D. Simple method for reduction of autofluorescence in fluorescence microscopy. J Histochem Cytochem. 2002;50(3):437–9. https://doi.org/10.1177/002215540205000315

6. Qi L, Knapton EK, Zhang X, Zhang T, Gu C, Zhao Y. Pre-culture Sudan black B treatment suppresses autofluorescence signals emitted from polymer tissue scaffolds. Sci Rep. 2017;7(1):8361. https://doi.org/10.1038/s41598-017-08723-2
7. Rebenku I, Lloyd CB, Szollosi J, Vereb G. Pixel-by-pixel autofluorescence corrected FRET in fluorescence microscopy improves accuracy for samples with spatially varied autofluorescence to signal ratio. Sci Rep. 2023;13(1):2934. https://doi.org/10.1038/s41598-023-30098-w
8. Rigacci L, Alterini R, Bernabei PA, Ferrini PR, Agati G, Fusi F, et al. Multispectral imaging autofluorescence microscopy for the analysis of lymph-node tissues. Photochem Photobiol. 2000;71(6):737–42. https://doi.org/10.1562/0031-8655(2000)071<0737:miamft>2.0.co;2
9. Sebestyen Z, Nagy P, Horvath G, Vamosi G, Debets R, Gratama JW, et al. Long wavelength fluorophores and cell-by-cell correction for autofluorescence significantly improves the accuracy of flow cytometric energy transfer measurements on a dual-laser benchtop flow cytometer. Cytometry. 2002;48(3):124–35. https://doi.org/10.1002/cyto.10121
10. Ferrer-Font L, Small SJ, Lewer B, Pilkington KR, Johnston LK, Park LM, et al. Panel optimization for high-dimensional immunophenotyping assays using full-spectrum flow cytometry. Curr Protoc. 2021;1(9):e222. https://doi.org/10.1002/cpz1.222
11. Bertolo A, Baur M, Guerrero J, Pötzel T, Stoyanov J. Autofluorescence is a reliable in vitro marker of cellular senescence in human mesenchymal stromal cells. Sci Rep. 2019;9(1):2074. https://doi.org/10.1038/s41598-019-38546-2
12. Yang Y, Yu Q, Li B, Li S, Yang Z, Yuan F, et al. A single dose of lipopolysaccharide elicits autofluorescence in the mouse brain. Front Aging Neurosci. 2023;15:1126273. https://doi.org/10.3389/fnagi.2023.1126273
13. Moran C, Munch G, Forbes JM, Beare R, Blizzard L, Venn AJ, et al. Type 2 diabetes, skin autofluorescence, and brain atrophy. Diabetes. 2015;64(1):279–83. https://doi.org/10.2337/db14-0506
14. Komura T, Yamanaka M, Nishimura K, Hara K, Nishikawa Y. Autofluorescence as a noninvasive biomarker of senescence and advanced glycation end products in *Caenorhabditis elegans*. NPJ Aging Mech Dis. 2021;7(1):12. https://doi.org/10.1038/s41514-021-00061-y
15. Novo D. A comparison of spectral unmixing to conventional compensation for the calculation of fluorochrome abundances from flow cytometric data. Cytometry A. 2022;101(11):885–91. https://doi.org/10.1002/cyto.a.24669
16. Kharraz Y, Lukesova V, Serrano AL, Davison A, Munoz-Canoves P. Full spectrum cytometry improves the resolution of highly autofluorescent biological samples: identification of myeloid cells in regenerating skeletal muscles. Cytometry A. 2022;101(10):862–76. https://doi.org/10.1002/cyto.a.24568
17. Jameson VJ, Luke T, Yan Y, Hind A, Evrard M, Man K, et al. Unlocking autofluorescence in the era of full spectrum analysis: implications for immunophenotype discovery projects. Cytometry A. 2022;101(11):922–41. https://doi.org/10.1002/cyto.a.24555
18. Fletcher AL, Malhotra D, Acto SE, Lukacs-Kornek V, Bellemare-Pelletiez A, Curry M, Armant M, Turley SJ. Reproducible isolation of lymph node stromal cells reveals site-dependent differences in fibroblastic reticular cells. Front Immunol. 2011;2:35. https://doi.org/10.3389/fimmu.2011.00035
19. Park LM, Lannigan J, Jaimes MC. OMIP-069: forty-color full Spectrum flow cytometry panel for deep immunophenotyping of major cell subsets in human peripheral blood. Cytometry A. 2020;97(10):1044–51. https://doi.org/10.1002/cyto.a.24213
20. Jensen HA, Kim J. iCoreDrop: a robust immune monitoring spectral cytometry assay with six open channels for biomarker flexibility. Cytometry A. 2023;103(5):405–18. https://doi.org/10.1002/cyto.a.24708
21. Peixoto MM, Soares-da-Silva F, Schmutz S, Mailhe MP, Novault S, Cumano A, et al. Identification of fetal liver stroma in spectral cytometry using the parameter autofluorescence. Cytometry A. 2022;101(11):960–9. https://doi.org/10.1002/cyto.a.24567
22. Bertolo A, Guerrero J, Stoyanov J. Autofluorescence-based sorting removes senescent cells from mesenchymal stromal cell cultures. Sci Rep. 2020;10(1):19084. https://doi.org/10.1038/s41598-020-76202-2
23. Dorward DA, Lucas CD, Alessandri AL, Marwick JA, Rossi F, Dransfield I, et al. Technical advance: autofluorescence-based sorting: rapid and nonperturbing isolation of ultrapure neutrophils to determine cytokine production. J Leukoc Biol. 2013;94(1):193–202. https://doi.org/10.1189/jlb.0113040
24. Jong TAD, Semmelink JF, Bolt JW, Grasso C, Hoebe RA, Krawczyk PM, et al. Senescence phenotype of lymph node stromal cells from patients with rheumatoid arthritis is partly restored by dasatinib treatment. bioRxiv. 2023. https://doi.org/10.1101/2023.12.10.571042
25. Erben T, Ossig R, Naim HY, Schnekenburger J. What to do with high autofluorescence background in pancreatic tissues—an efficient Sudan black B quenching method for specific immunofluorescence labelling. Histopathology. 2016;69(3):406–22. https://doi.org/10.1111/his.12935
26. Sun Y, Yu H, Zheng D, Cao Q, Wang Y, Harris D, et al. Sudan black B reduces autofluorescence in murine renal tissue. Arch Pathol Lab Med. 2011;135(10):1335–42. https://doi.org/10.5858/arpa.2010-0549-OA
27. Tsuneoka Y, Atsumi Y, Makanae A, Yashiro M, Funato H. Fluorescence quenching by high-power LEDs for highly sensitive fluorescence in situ hybridization. Front Mol Neurosci. 2022;15:976349. https://doi.org/10.3389/fnmol.2022.976349
28. Kwok SJJ, Forward S, Fahlberg MD, Cosgriff S, Lee SH, Abbott G, et al. Laser particle barcoding for multi-pass high-dimensional flow cytometry. bioRxiv. 2022;8(3):310–24. https://doi.org/10.1101/2022.06.03.494697
29. Mair F, Tyznik AJ. High-dimensional immunophenotyping with fluorescence-based cytometry: a practical guidebook. Methods Mol Biol. 2019;2032:1–29. https://doi.org/10.1007/978-1-4939-9650-6_1

SUPPORTING INFORMATION

Additional supporting information can be found online in the Supporting Information section at the end of this article.

How to cite this article: Roet JEG, Mikula AM, de Kok M, Chadick CH, Garcia Vallejo JJ, Roest HP, et al. Unbiased method for spectral analysis of cells with great diversity of autofluorescence spectra. Cytometry. 2024. https://doi.org/10.1002/cyto.a.24856